Available online at www.sciencedirect.com
SCIENCE DIRECT®
International Journal of Machine Tools & Manufacture 43 (2003) 1437–1446
INTERNATIONAL JOURNAL OF MACHINE TOOLS & MANUFACTURE DESIGN, RESEARCH AND APPLICATION

Prediction of regenerative chatter by modelling and analysis of high-speed milling

R.P.H. Faassen [a,*], N. van de Wouw [a], J.A.J. Oosterling [b], H. Nijmeijer [a]

[a] *Department of Mechanical Engineering, Eindhoven University of Technology, P.O. Box 513, 5600 MB Eindhoven, The Netherlands*
[b] *Manufacturing Development, TNO Institute of Industrial Technology, P.O. Box 6235, 5600 HE Eindhoven, The Netherlands*

Received 19 March 2003; received in revised form 16 June 2003; accepted 17 June 2003

Abstract

High-speed milling is widely used in the manufacturing industry. For the efficiency of the milling process, high demands on the material removal rate and the surface generation rate are posed. The process parameters, determining these two rates, are restricted by the occurrence of regenerative chatter. Chatter is an undesired instability phenomenon, which causes both a reduced product quality and rapid tool wear. In this paper, the milling process is modelled, based on dedicated experiments on both the material behaviour of the workpiece material and the machine dynamics. These experiments show that both the material properties and the machine dynamics are dependent on the spindle speed. Furthermore, a method for the prediction of the chatter boundaries is proposed and applied in order to predict the chatter boundaries as a function of process parameters, such as spindle speed and depth-of-cut, for spindle speed varying material and machine parameters. Finally, experiments are performed to estimate these chatter boundaries in practice. The modelled chatter boundaries are compared to the experimental results in order to validate the model and the stability analysis.

Keywords: High-speed milling; Regenerative chatter; Machine dynamics; *D*-partitioning method; Stability

1. Introduction

In the present manufacturing industry, the high-speed milling process plays an important role. Some examples are the fabrication of moulds and the aeroplane building industry, where large amounts of material are removed from a large structure. The milling process is most efficient if the material removal rate is as large as possible, while maintaining a high quality level. For a certain machine–tool–workpiece combination, the main factors that influence this removal rate are the spindle speed, the depth-of-cut (axial and radial) and the feed rate.

During the milling process, chatter can occur at certain combinations of axial depth-of-cut and spindle speed. This is an undesired phenomenon, since the surface of the workpiece becomes non-smooth as a result of heavy vibrations of the cutter. Moreover, the cutting tool and machine wear out rapidly and a lot of noise is produced when chatter occurs. Several physical mechanisms causing chatter can be distinguished [21]. Wiercigroch et al. [20,22] and Grabec [5] showed that friction between the tool and workpiece can cause chatter. Chatter can also be caused by the thermodynamics of the cutting process [4,21]. In [16], the phenomenon of mode-coupling is discussed as a cause of chatter. Chatter due to these physical mechanisms is often called primary chatter. Secondary chatter is caused by the regeneration of waviness of the surface of the workpiece. This so-called regenerative chatter is considered to be one of the most important causes of instability in the cutting process. This type of chatter will be considered in this paper.

Several studies have been performed since the late 1950s regarding regenerative chatter, by e.g. Tobias and Fishwick [18,19], Tlusty and Polacek [17], Merrit [10] and Altintas [1]. It was shown that the border between a stable cut (i.e. no chatter) and an unstable cut (i.e. with chatter) can be visualized in terms of the axial depth-of-

* Corresponding author. Tel.: +31-40-247-5730; fax: +31-40-246-1418.
E-mail address: r.p.h.faassen@tue.nl (R.P.H. Faassen).

0890-6955/$ - see front matter © 2003 Elsevier Ltd. All rights reserved.
doi:10.1016/S0890-6955(03)00171-8

cut as a function of the spindle speed. This results in a stability lobes diagram (SLD). Using these diagrams it is possible to find the specific combination of machining parameters, which results in the maximum chatter-free material removal rate.

In order to predict the stability boundaries related to chatter, an accurate dynamic model for the milling process is needed. Various models have been suggested by e.g. Tlusty [16], Altintas [1] and Insperger and Stépán [6]. Despite the differences between these models, they all use parameters to describe the cutting process and machine dynamics, that are constant for the full spindle speed range under consideration. This means that dependencies of the dynamic behaviour of the milling machine or the cutting process on the spindle speed are not modelled. To investigate such dependencies, dedicated experiments have to be performed. Furthermore, a different model should be used, to account for these dependencies. In order to construct stability lobes using this model, a method which is capable of handling spindle speed varying model parameters is necessary.

In Section 2, the modelling of the milling process is described. The model consists of a part which describes the machine–tool interaction and a part which describes the machine dynamics. For both model parts, dedicated experiments are performed to support such modelling for a large spindle speed range. Based on these experiments, it can be concluded that the parameters of this model are dependent on the spindle speed. Furthermore, a material model has been used which can predict the dependency of the stability lobes on the feed rate. The resulting model is described by a set of linear delay differential equations. In Section 3, the *D*-partitioning method [12,14] is used to analyse the stability boundary, in terms of spindle speed and depth-of-cut, of the equilibrium point (reflecting a stable cut) of those differential equations. This method can also be used for spindle speed dependent model parameters. The results of such a stability analysis for the model, constructed in Section 2, is compared to experimentally determined stability boundaries in Section 4 for validation purposes. Finally in Section 5, conclusions are presented.

2. Modelling

In the milling process, material is removed from a workpiece by a rotating cutting tool. While the tool rotates, it translates in the feed direction at a certain speed. A schematic representation of the milling process is shown in Fig. 1. The process parameters shown are the spindle speed Ω, the feed per tooth (also called chip load) f_z, the radial depth-of-cut a_e and the axial depth-of-cut a_p. The chip thickness is not constant, but periodic, as a result of the feed rate and the rotation of the cutter.

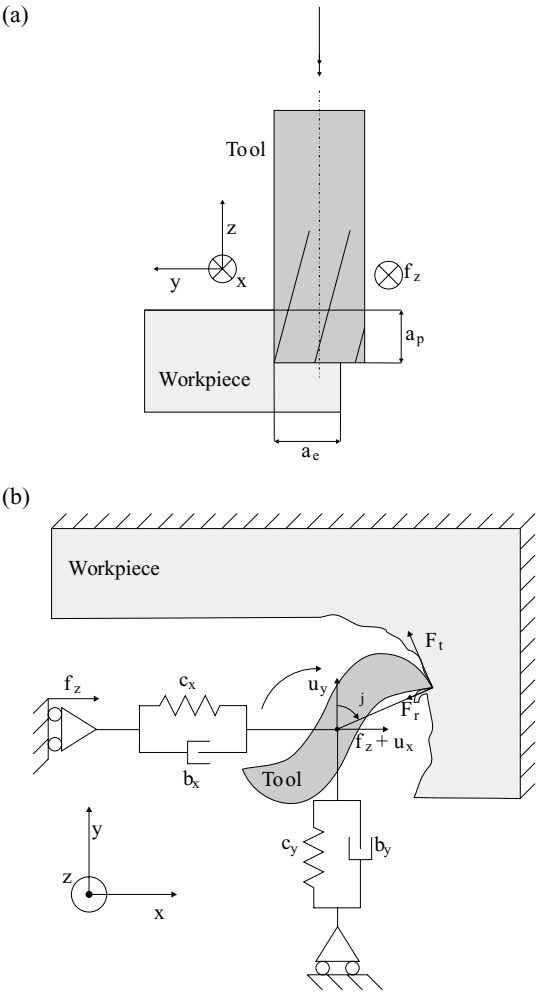

Fig. 1. Schematic representation of the milling process.

The milling process is an interaction between the tool and the workpiece. This is shown in the block diagram of Fig. 2. A certain displacement of the cutter, related to the feed and rotation angle, is dictated to the spindle. This displacement results in the static chip thickness h_{stat}. In order to achieve this displacement, the cutter encounters a resistance force **F** due to the workpiece–tool interaction, if the cutter is actually in cut. This resistance force results in a displacement of the cutter **u**, which causes a difference between the prescribed displacement and the actual displacement of the cutter.

The mechanism described above results in vibrations of the tool, which cause a wavy surface on the workpiece. The next tooth in cut encounters this wavy surface and generates its own wavy surface. The chip thickness is, therefore, the sum of the static and dynamic chip thickness. The static chip thickness is the result of the feed per tooth f_z and the rotation angle of the cutting tooth ϕ:$h_{stat}(t) = f_z \sin(\phi(t))$, where the cutting path is assumed to be a circular arc. The dynamic chip thickness is a function of the vibration of the tooth in x and y direction, see Fig. 1, and the vibration of the previous

tooth in these directions. These displacement coordinates are gathered in a displacement column $\mathbf{u} = [u_x \; u_y]^T$. The dynamic chip thickness can now be described as $h_{dyn}(t) = [\sin(\phi(t)) \; \cos(\phi(t))](\mathbf{u}(t)-\mathbf{u}(t-\tau))$. The tooth passing period time determines the delay time τ in Fig. 2. Given the spindle speed Ω in rpm and z the number of teeth on the cutter, the tooth passing period time is defined as

$$\tau = \frac{60}{z\Omega}. \tag{1}$$

Appropriate modelling of the cutting process and machine dynamics (see Fig. 2) is discussed in Sections 2.1 and 2.2, respectively.

2.1. Material model

As mentioned in Section 2, the milling process is an interaction between the cutting process and the milling dynamics. In this section, the focus lies on the cutting process. In literature, various models have been proposed to model the tangential and radial cutting forces F_t and F_r as a function of the cutting parameters, such as the depth-of-cut and the feed per tooth. For some of these models, the forces acting on a single cutting tooth are shown in Table 1. The parameter $K_{c1.1}$ in the model by Kienzle, is defined as the force that is needed to cut a chip of 1-by-1 mm.

As was stated before, the static chip thickness is approximated by $h_{stat} = f_z \sin\phi_j$, where ϕ_j is the rotation angle of tooth j. The dynamic chip thickness is assumed to be the difference between the vibration of the current tooth, determined by $u_x(t)$, $u_y(t)$ and $\phi_j(t)$, and the vibration of the previous tooth, determined by $u_x(t-\tau)$, $u_y(t-\tau)$ and $\phi_{j-1}(t-\tau)$, where $\phi_j(t) = \phi_{j-1}(t-\tau)$. Consequently, the chip thickness h encountered by tooth j can be described as a function of rotation angle ϕ_j by $h = h_{stat} + h_{dyn}$:

$$h_j(\phi_j(t)) = f_z \sin\phi_j(t) + (u_x(t)-u_x(t-\tau))\sin\phi_j(t) + (u_y(t)-u_y(t-\tau))\cos\phi_j(t), \tag{2}$$

with

$$\phi_j(t) = \Omega\, t + j\,\vartheta, \quad j = 0,1,\ldots,z-1, \tag{3}$$

where Ω is expressed in rad/s and $\vartheta = 2\pi/z$ is the angle between two subsequent teeth. The radial and tangential forces are zero when the tooth is not in cut. This can be modelled by multiplying the equations which describe the force of Table 1 by a function $g_j(\phi_j(t))$, that describes whether a tooth is in or out of cut. The tooth is in cut if $\phi_s \le \phi_j \le \phi_e$, where ϕ_s and ϕ_e are the start and exit angles, respectively. This function is given by [6]:

$$g_j(\phi_j(t)) = \frac{1}{2}(1 + \text{sign}(\sin(\phi_j(t)-\psi)-p)) = \begin{cases} 1, & \phi_s \le \phi_j(t) \le \phi_e \\ 0, & \text{else} \end{cases}, \tag{4}$$

with

$$\tan\psi = \frac{\sin\phi_s - \sin\phi_e}{\cos\phi_s - \cos\phi_e}, \quad p = \sin(\phi_s - \psi). \tag{5}$$

In Table 1, both linear and exponential functions of the chip thickness are shown. The main advantage of an exponential model, is the fact that the stability lobes calculated using such a model are feed rate dependent. For a fixed spindle speed Ω, at low chip loads (0.08 or 0.12 mm/tooth) chatter can occur, while at the same spindle speed for higher chip loads, chatter does not occur. This behaviour was found in practice, performing the experiments discussed later in this section, and cannot be predicted using a linear model. The model used in this paper is an exponential model, where a constant term has been added. This term adds the effect of "ploughing" or "rubbing" at the flank of the cutting edge [1]. For a single tooth, the tangential and radial force are given by:

$$F_{t_j}(t) = (K_t a_p h_j(t)^{x_F} + K_{te} a_p) g_j(\phi_j(t)), \tag{6}$$

$$F_{r_j}(t) = (K_r a_p h_j(t)^{x_F} + K_{re} a_p) g_j(\phi_j(t)), \tag{7}$$

where $0 < x_F < 1$, $K_t, K_r > 0$ and $K_{te}, K_{re} \ge 0$. Using (2), (4) and (6), the cutting forces can be described as

$$\underline{F}(t) = \begin{bmatrix} F_x(t) \\ F_y(t) \end{bmatrix} = a_p \sum_{j=0}^{x-1} g_j(\phi_j(t)) \left(\begin{bmatrix} -K_{te}\cos\phi_j(t) - K_{re}\sin\phi_j(t) \\ +K_{te}\sin\phi_j(t) - K_{re}\cos\phi_j(t) \end{bmatrix} + (f_z \sin\phi_j(t) + u_x(t,t-\tau)\sin\phi_j(t) + u_y(t,t-\tau)\cos\phi_j(t))^{x_F} \cdot \begin{bmatrix} -K_t\cos\phi_j(t) - K_r\sin\phi_j(t) \\ +K_t\sin\phi_j(t) - K_r\cos\phi_j(t) \end{bmatrix} \right) \tag{8}$$

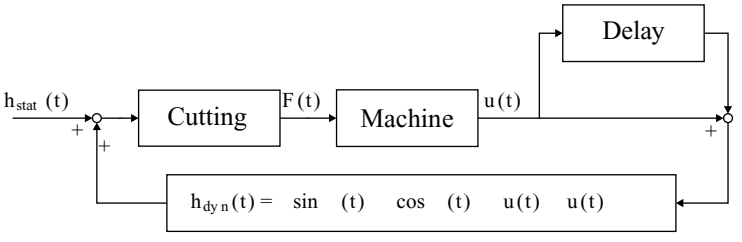

Fig. 2. Block diagram of the milling process.

Table 1
Different models for the cutting force

Author (group)	Model	Year
Kienzle and Victor [7]	$\bar{F}_t = a_p K_{c1.1} \bar{h}^{1-m}$	1950s
Altintas [1,2]	$F_t = a_p K_{tc} h + a_p K_{te}$ $F_r = a_p K_{rc} h + a_p K_{re}$	1990s, 2000s
Stépán [6,15]	$F_t = a_p K_t h^{x_F}$ $F_r = a_p K_r h^{x_F}$	1990s, 2000s

with $\mathbf{u}(t,t-\tau) = \mathbf{u}(t) - \mathbf{u}(t-\tau)$. This equation can also be linearized around $\mathbf{u} = 0$, which corresponds to a cut where no vibrations occur, hence a stable cut without chatter. This results in $\mathbf{F} = \mathbf{F}(\mathbf{u} = 0) + \Delta\mathbf{F}$. The linearized force $\Delta\mathbf{F}$ can then be written as:

$$\Delta\mathbf{F} = a_p \underline{k}(t)\mathbf{u}(t,t-\tau), \tag{9}$$

with the matrix $\underline{k}(t)$ defined by

$$\underline{k}(t) = \begin{bmatrix} k_{xx} & k_{xy} \\ k_{yx} & k_{yy} \end{bmatrix} = \sum_{j=0}^{z-1} f_z^{x_F - 1} x_F g_j(\phi_j(t)) s^{x_F} \cdot \begin{bmatrix} -(K_t c + K_r s) & -s^{-1}c(K_t c + K_r s) \\ +(K_t s - K_r c) & +s^{-1}c(K_t s - K_r c) \end{bmatrix}, \tag{10}$$

where $s = \sin\phi_j(t)$ and $c = \cos\phi_j(t)$. It can be seen that the parameters K_{te} and K_{re} disappear in this linearization. However, including these parameters in the definition of the model (6), gives the advantage to fit the model to the experimentally found values more accurately, as will be shown in Fig. 4, later in this section. It can also be seen that the feed per tooth f_z is explicitly included in this equation. This is a result of the choice of the exponential model. Should a linear model have been used, i.e. $x_F = 1$, the feed per tooth f_z disappears from Eq. (10).

If the spindle dynamics can be modelled as a linear mass–spring–damper system, the milling process described by the block diagram in Fig. 2, obeys:

$$\underline{M}\ddot{\mathbf{u}}(t) + \underline{B}\dot{\mathbf{u}}(t) + \underline{C}\mathbf{u}(t) = a_p \underline{k}(t)\mathbf{u}(t,t-\tau), \tag{11}$$

with $\underline{M}$, $\underline{B}$ and $\underline{C}$ the mass, damping and stiffness matrices, respectively. It should be noted that, in Section 2.2, a higher-order model for the machine dynamics is constructed.

In order to identify the parameters K_t, K_r, K_{te}, K_{re} and x_F of the model described above, dedicated experiments are performed. A schematic representation of the experimental setup is shown in Fig. 3. An aluminium 6082 workpiece is mounted on a dynamometer type Kistler 9255. Using this dynamometer and a charge amplifier, the forces in x, y and z direction, can be measured. The dynamometer is placed on the machine bed in such a way that x is the feed direction, y is the normal direction and z the axial direction. At full immersion (i.e. $\phi_s = 0°$ and $\phi_e = 180°$), a cut is made and the forces are measured. The cuts have been made using a Mikron HSM 700 milling machine and a two-teeth, 10 mm diameter Jabro Tools JH420 cutter mounted in a Kelch shrink-fit toolholder. The spindle speed has been varied from 15 000 to 40 000 rpm with increments of 5000 rpm. At each spindle speed, the feed per tooth has been varied from 0.08 to 0.24 mm/tooth with increments of 0.04 mm/tooth. Two cuts have been made at each combination of spindle speed and feed per tooth.

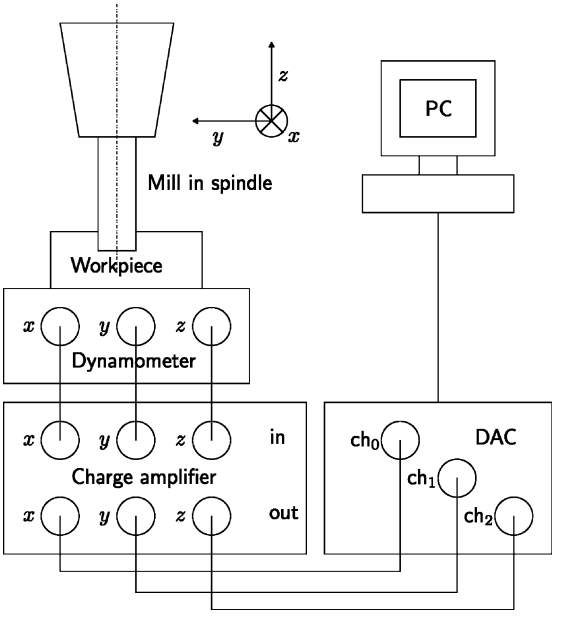

Fig. 3. Schematic representation of the setup for the cutting experiments.

At each experiment, the mean cutting forces, $\bar{F}_x = \int_0^\tau F_x(t)\mathrm{d}t$, $\bar{F}_y = \int_0^\tau F_y(t)\mathrm{d}t$, have been calculated. When performing the experiments, a helical end mill has been

Table 2
Material parameters for cutting at 15 000 rpm

K_t	462	N/mm^{1+x_F}
K_{te}	2.19×10^{-6}	N/mm
K_r	38.6	N/mm^{1+x_F}
K_{re}	20.5	N/mm
x_F	0.744	–

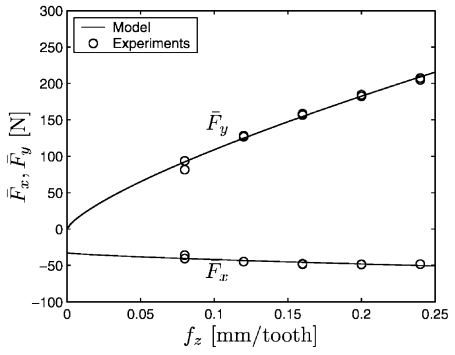

Fig. 4. Estimated and measured mean forces at 15 000 rpm. Material parameters can be found in Table 2.

used. Since the total amount of material removed is independent of the helix angle, the material parameters are independent of the helix angle [1]. At each spindle speed, the exponential model has been fitted onto those mean cutting forces using a least squares estimation procedure, as is shown in Fig. 4 for a spindle speed of 15 000 rpm. (At each spindle speed two cuts have been made at five different chip loads. These 10 measurements have been used to fit the material parameters for this particular spindle speed.) The material parameters of this exponential model can be found in Table 2.

The corresponding measured forces and modelled forces, at a feed per tooth of 0.16 mm/tooth, are shown in Fig. 5. If the spindle speed is changed, also the values for the material parameters change to a certain extent. In Fig. 6, the material parameters are shown as a function of spindle speed.

2.2. Machine model

The second part of the block diagram of Fig. 2 represents the modelling of the machine dynamics, i.e. the tool, toolholder and spindle. In this section, the machine dynamics will be modelled based on dedicated experiments.

In literature [3,8,11], the machine system is assumed

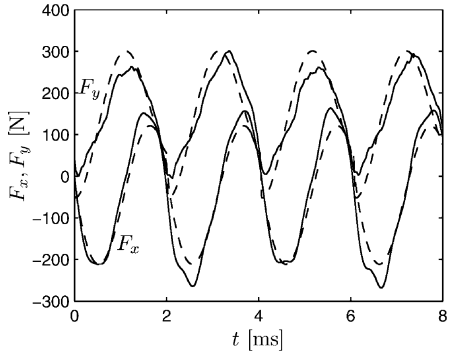

Fig. 5. Forces in x and y direction as a function of time at 15 000 rpm and a feed per tooth of f_z = 0.16 mm/tooth (solid: experiments; dashed: model).

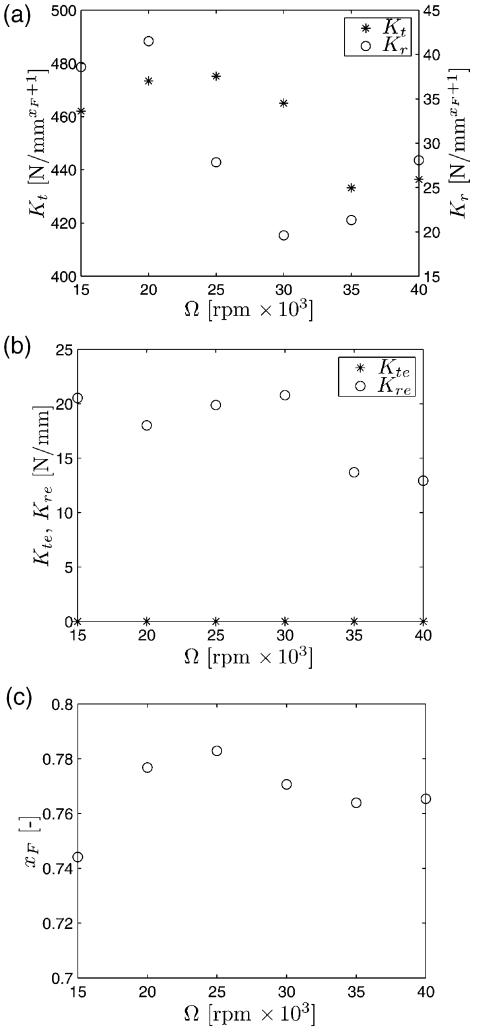

Fig. 6. Material parameters of the exponential model as a function of spindle speed.

to be a 1DOF or 2DOF linear second-order (mass–spring–damper) system. However, experiments will show that a higher-order model is necessary to describe the machine dynamics. The dynamics can be described by the transfer function matrix between cutting forces $\mathbf{F} = [F_x \; F_y]^{\mathrm{T}}$ and displacements of the cutter $\mathbf{u} = [u_x \; u_y]^{\mathrm{T}}$:

$$\mathbf{U}(s) = \underline{H}_{\mathbf{uF}}(s)\mathbf{F}(s) = \begin{bmatrix} H_{xx}(s) & H_{xy}(s) \\ H_{yx}(s) & H_{yy}(s) \end{bmatrix} \mathbf{F}(s), \tag{12}$$

where $\mathbf{U}(s) = \mathscr{L}(\mathbf{u}(t))$ and $\mathbf{F}(s) = \mathscr{L}(\mathbf{F}(t))$, with $\mathscr{L}(\cdot)$ the Laplace operator.

Each entry of this transfer function matrix can be modelled using the following model form:

$$H_{ij}(s) = \left(\frac{b_m s^m + b_{m-1} s^{m-1} + \ldots + b_1 s + b_0}{a_n s^n + a_{n-1} s^{n-1} + \ldots + a_1 s + a_0} \right)_{ij}, \tag{13}$$

where the coefficients a and b differ for different i and j. It will be assumed that $H_{ij} = 0$ for $i \neq j$. In other

words, the dynamics in x and y direction is decoupled. These transfer functions describe the dynamics of the cutter (mill), due to flexibility of the mill, and the dynamics of the spindle and toolholder, from now on called the spindle dynamics. Firstly, experiments are performed to measure the spindle dynamics at different spindle speeds. Secondly, experiments are performed, at $\Omega = 0$ rpm, to measure the dynamics of the mill. Let us now discuss these experiments performed to retrieve H_{xx} and H_{yy}.

In order to measure the dynamic behaviour of the spindle system, consisting of the tool, toolholder and spindle, and the influence of the spindle speed on this dynamic behaviour, impulse tests are performed. Using the results of these tests, it is possible to find a frequency response function between the force applied to the tool and the displacement of the tool, which provides information on the dynamical behaviour of the spindle system. These impulse tests are performed at various spindle speeds, in order to study the spindle speed dependency of the machine dynamics. A schematic representation of the setup is shown in Fig. 7. A 50 mm long, 10 mm diameter carbide cylinder is mounted on a Kelch shrink-fit toolholder and used on a Mikron HSM 700 milling machine. Since the spindle is rotating while being hit by the impulse hammer, a mill cannot be used. The first natural frequency of the cylinder is approximately 4 kHz and the dynamics of toolholder and spindle is related to a lower frequency range. Therefore, the dynamics of the toolholder and spindle can be distinguished from the dynamics of the cylinder and identified separately.

The displacement of the cylinder in x or y direction is measured with an LMI Laser Twin Sensor (LTS 15/3). An impulse force hammer is used to hit the cylinder and to measure the force applied to it. A Siglab dynamic signal analyser is used for data acquisition purposes. The spindle speed has been varied from 0 to 25 000 rpm, with increments of 5000 rpm. At each spindle speed, 20 impacts have been performed in both x and y direction, while the laser has been placed opposite to the place of impact.

In Fig. 8, the absolute value of the measured frequency response function $H_{xx}(i\omega)$ is depicted at different spindle speeds (mean of 20 measurements). Statistical significance tests showed that the differences between these frequency response functions at different spindle speeds are significant, especially in the frequency range of 750–1750 Hz, in which the most important resonances related to the spindle dynamics are situated. Since the natural frequency of the cylinder lies in the order 4 kHz and the measured natural frequencies are much lower, the latter frequencies are not the natural frequencies of the cylinder but are related to the toolholder and spindle. Identical experiments are performed to measure $H_{yy}(i\omega)$.

Next, the same type of experiments are performed on a non-rotating mill in order to capture the dynamics of the real cutter tool. Since the flexibility modes of the tool do not depend on the spindle speed, only measurements at 0 rpm are performed. The total dynamics of the toolholder and spindle and the mill can now be constructed by superposition of the individual dynamics of the toolholder and spindle on the one hand and the dynamics of the mill on the other hand, see Fig. 9. In doing so, up to 2530 Hz the spindle dynamics is taken into account and above 2530 Hz the mill dynamics is dominant.

The total machine dynamics, see Fig. 9, can now be

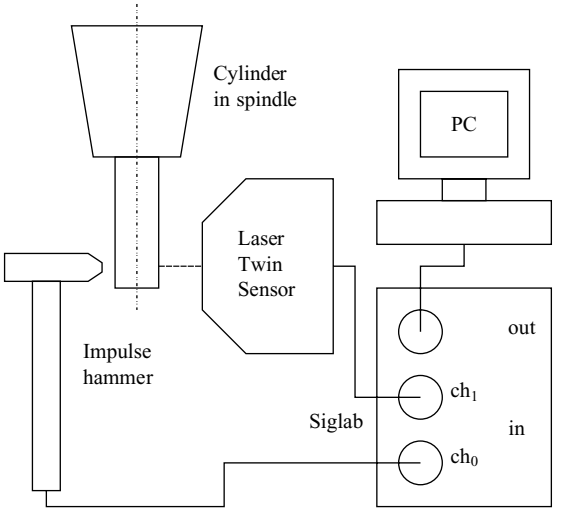

Fig. 7. Schematic representation of the setup for the impulse tests.

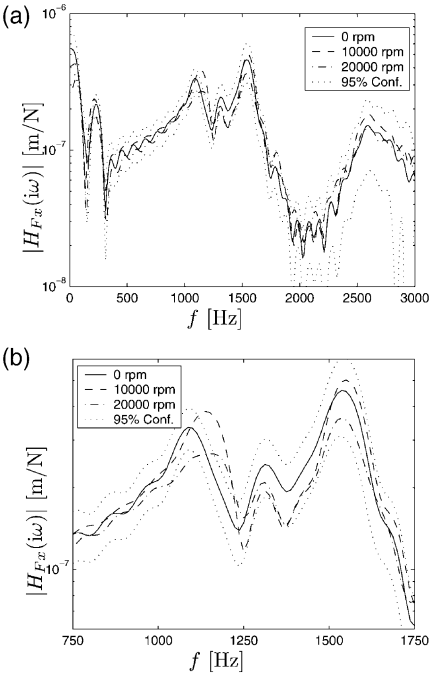

Fig. 8. $|H_{xx}|$ at different spindle speeds Ω. Dotted line: 95% confidence interval at 0 rpm.

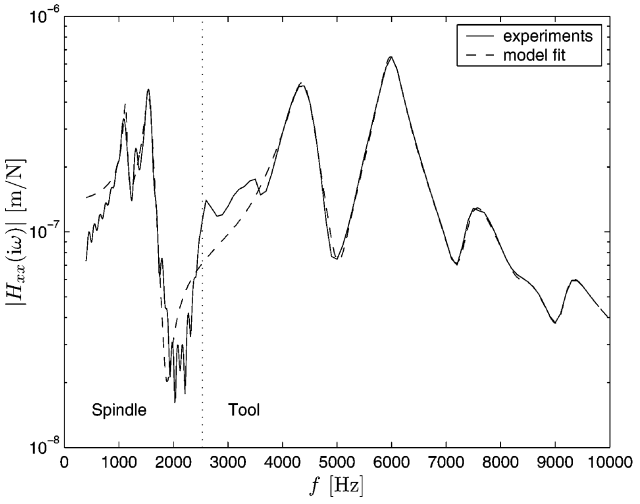

Fig. 9. Measured $|H_{xx}|$ for $\Omega = 0$ rpm incorporating both tool dynamics and toolholder and spindle dynamics.

modelled using (12) and (13). In order to obtain the parameters of this model, the distance between the measured and modelled frequency response functions in the complex plane is minimized using an optimization routine and a least squares type object function. In Fig. 9, the resulting modelled frequency response function H is compared to the measured frequency response function, for $\Omega = 0$. When performing this identification step, the highest level of importance was assigned to the highest resonance peaks in the absolute value of the experimental frequency response function, because these resonances are dominant in the stability analysis, as will be shown in Section 4. Of course, the same parametric identification procedure was performed for other spindle speeds, resulting in different dynamic models at different spindle speeds.

2.3. The total milling model

The models for the material behaviour and the dynamics of tool, toolholder and spindle can be combined to form a model for the milling process using the block diagram of the milling process as depicted in Fig. 2. This leads to the following description of the milling process in the Laplace domain:

$$\underline{H}_{\mathbf{uF}}^{-1}(s)\mathbf{U}(s) = a_p\underline{K}(s)*(1-e^{-s\tau})\mathbf{U}(s), \tag{14}$$

where $\underline{H}_{\mathbf{uF}}(s)$ is defined by (12) and (13), the matrix $\underline{K}(s) = \mathscr{L}(\underline{k}(t))$ is the Laplace transform of the matrix $\underline{k}(t)$ related to the material properties, and '$*$' denotes the convolution operator.

It should be noted that (14) represents the Laplace transform of a set of linear non-autonomous delay differential equations, where the non-autonomous nature is due to the explicit time-dependency of $\underline{k}(t)$. For the remainder of this paper, $\underline{k}(t)$ will be approximated by its zero-th order Fourier approximation:

$$\underline{k} = \frac{1}{\tau}\int_0^{\tau}\underline{k}(t)\mathrm{d}t \tag{15}$$

which, since $\underline{k}(t)$ is only non-zero if a tooth is actually in cut, equals

$$\underline{k} = \frac{1}{\vartheta}\int_{\phi_s}^{\phi_e}\underline{k}(\phi)\mathrm{d}\phi, \tag{16}$$

where ϑ is the angle between two subsequent teeth, $\phi = \Omega t$ and $\underline{k}(t)$ is defined by (10) for the linearized exponential material model. This approximation is quite common in literature and dramatically simplifies the stability analysis since it transforms the model into an autonomous model [1]. Consequently, the convolution operation in (14) changes to a normal multiplication:

$$\underline{H}_{\mathbf{uF}}^{-1}(s)\mathbf{U}(s) = a_p\underline{K}(1-e^{-s\tau})\mathbf{U}(s). \tag{17}$$

where $\underline{K}$ is a constant matrix.

3. Stability analysis of the milling system

In this section, the model of the milling system proposed in the previous section (see (17)) will be used for the purpose of stability analysis. The linear autonomous delay differential equation describing the dynamics of (17) in the time-domain exhibits one unique equilibrium point: $\mathbf{u} = 0$, which corresponds to the desired no-chatter situation. Therefore, the stability of this equilibrium point corresponds to the stability of the milling process and instability of the equilibrium point corresponds to a response with chatter.

Here, the method of D-partitioning [12] will be used to assess the stability of this equilibrium point. This method was used by, e.g. Stépán [13,14] to investigate the stability of the milling process using a single-degree-of-freedom, single-mode milling model. Note that, for a given spindle speed Ω, the stability of the equilibrium point depends on the axial depth-of-cut a_p. So, the stability analysis will aim at finding the critical value for a_p, at a given spindle speed Ω, which forms the stability boundary, allowing for the construction of so-called stability lobes diagrams.

The method of D-partitioning uses the criterion that an equilibrium point of a system, described by a linear, autonomous delay differential equation, is asymptotically stable if and only if all the roots of its characteristic equation lie in the open left-half complex plane. It should be noted that a delay-differential equation has an infinite number of poles. The characteristic equation corresponding to (17) is given by

$$\det(\underline{H}_{\mathbf{uF}}^{-1}(s) - a_p\underline{K}(1-e^{-s\tau})) = 0. \tag{18}$$

A certain choice for the systems parameters (in this case a_p) determines the number of poles in the open left-half complex plane. The parameter space can be divided into domains $D(k,n-k)$, $0 \leq k \leq n$ which contains all the points with poles with k negative real parts and n–k positive real parts. This is called D-partitioning. The domain of asymptotic stability is the domain $D(n, 0)$. An increase of the number of roots with positive real parts can occur if and only if a certain pole crosses the imaginary axis from the left to the right. This corresponds with the situation that a certain point in parameter space moves from the domain $D(k,n-k)$ to $D(k-1,n-(k-1))$. Therefore, the borders of the D-partitions are the map of the imaginary axis $s = i\omega$, with $-\infty < \omega < +\infty$ on the parameter space.

Let us introduce a new complex variable $S = s\tau$ and use this to rewrite the characteristic Eq. (18) into

$$\det\left(\underline{H}_{\mathbf{uF}}^{-1}\left(\frac{S}{\tau}\right) - a_p \underline{K}(1-e^{-S})\right) = 0. \tag{19}$$

We will use this equation to determine the values for the parameter a_p for which at least one pole lies on the imaginary axis ($s = i\omega$). Using the fact that $\underline{H}_{\mathbf{uF}}(s)$ is given by (12), with $H_{xy} = H_{yx} = 0$, and choosing $S = i\omega^*$, with $\omega^* = \omega\tau$, which corresponds to $s = i\omega$, Eq. (19) transforms to

$$a_0 a_p^2 + a_1 a_p + 1 = 0, \tag{20}$$

with

$$a_0 = (1-\cos\omega^* + i\sin\omega^*)^2 H_{xx}(\omega^*) H_{yy}(\omega^*) (k_{xx}k_{yy} - k_{xy}k_{yx}), \tag{21}$$

$$a_1 = -(1-\cos\omega^* + i\sin\omega^*)(k_{xx}H_{xx}(\omega^*) + k_{yy}H_{yy}(\omega^*)). \tag{22}$$

The axial depth-of-cut as a function of $\omega*$, $a_p(\omega*)$, can then be found by

$$a_p(\omega^*) = \frac{-a_1 \pm \sqrt{a_1^2 - 4a_0}}{2a_0}. \tag{23}$$

The critical axial depth-of-cut (with respect to stability) is defined as the depth-of-cut a_p in the parameter set defined by $\{a_p(\omega^*):\mathrm{Im}a_p(\omega^*) = 0 \wedge \mathrm{Re}a_p(\omega^*) > 0\}$, for which $|\mathrm{Re}a_p(\omega^*)|$ has its minimum value, since for $a_p = 0$ all poles are in the open left-half complex plane when all the modes of the machine dynamics are damped, which is always the case in practice. The value for $\omega*$ for which this occurs, is the dimensionless chatter frequency $\omega^* = \omega_c^*$. The real chatter frequency that corresponds to the dimensionless chatter frequency is $\omega_c = \omega_c^*/\tau$. In summary, the following steps need to be taken in order to use the method of D-partitioning to find the chatter boundary in terms of a_p (for a specific value of the spindle speed):

(1) Choose a certain spindle speed Ω, and calculate the delay factor τ by Eq. (1);
(2) Choose a proper domain for ω^*;
(3) In the characteristic Eq. (19), substitute $S = i\omega^*$;
(4) Solve Eq. (20) for a_p. Now, $a_p(\omega*)$ is known, but $a_{p_{crit}}$ still has to be found;
(5) $\omega^* = \omega_c^*$ where $|\mathrm{Re}a_p(\omega_c^*)|$, in the parameter set defined by $\{a_p(\omega^*):\mathrm{Im}a_p(\omega^*) = 0 \wedge \mathrm{Re}a_p(\omega^*) > 0\}$, has its minimum value. By scanning the positive real axis, it is the point where a D-curve crosses the real axis for the first time. This is shown in Fig. 10. In this figure, the lines represent the boundaries between the domains $D(k,n-k)$;
(6) Calculate the chatter frequency $\omega_c = \omega_c^*/\tau$;
(7) Repeat all steps for different spindle speeds.

In the second step of this procedure, a choice for the domain of $\omega*$ should be made, such that ω_c^* lies in this domain. For a milling model, in which the lowest angular eigenfrequency of the machine dynamics is denoted by ω_l and the highest eigenfrequency by ω_h, a suitable choice for this domain is: $0.5\,\omega_l\tau < \omega^* < 1.5\,\omega_h\tau$.

4. Results

The model of the milling process, constructed in the previous section, will be used to pursue a stability analysis. Stability lobe diagrams can be computed using the analysis method illuminated in Section 3. In order to study the accuracy of the model, the stability boundaries obtained in this way need to be validated with the stability border determined in practice. The model used in this analysis uses the material model given in Section 2.1, where the material parameters are found by interpolating between the measured values at discrete spindle speeds as shown in Fig. 6. Moreover, the spindle speed dependency of the machine dynamics is taken into account in the following way. At discrete values for the spindle speed Ω, Ω = 0, 5000, 10 000, 15 000, 20 000, 25 000 rpm, models for the machine dynamics were con-

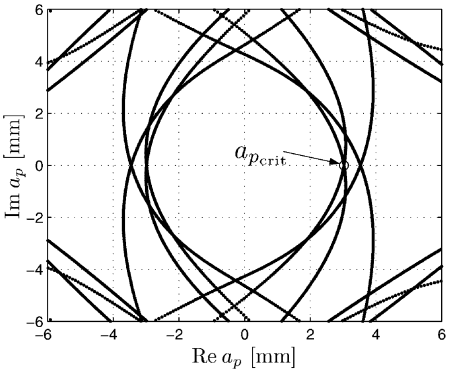

Fig. 10. D-partition diagram for a spindle speed of 25 024 rpm.

structed. When the stability analysis is performed for an arbitrary spindle speed (not at one of the discrete values for which the models were constructed) in order to find the critical value for the depth-of-cut a_p at that spindle speed, the dynamic model corresponding to the closest spindle speed is used. In this way, the spindle speed dependency of both the material and the machine dynamics is accounted for in the stability analysis. Taking this spindle speed dependency into account in determining the stability lobes demands for a method such as the *D*-partitioning method. The method, e.g. used by Altintas [1] cannot be used for an analysis, incorporating such spindle speed dependency of the model.

For validation purposes, the stability boundary, in terms of a_p as a function of Ω, has to be determined experimentally. Hereto, a series of cuts has been made at the Mikron HSM 700 milling machine using a two-teeth, 10 mm diameter Jabro Tools JH420 cutter mounted on a Kelch shrink-fit toolholder cutting an aluminium 6082 workpiece. For every spindle speed investigated, an initial depth-of-cut is chosen such that no chatter occurs. Whether chatter is occurring or not is detected using the experimental setup depicted in Fig. 11 and the software program Harmonizer [9]. This program scans the sound of the cutting process measured using the microphone. If the energy of the measured sound signal at a certain frequency exceeds a certain threshold, the cut is marked as exhibiting chatter. This threshold can be set automatically by Harmonizer, but it can also be set manually. Moreover, after the experiment, the generated surface of the workpiece is examined in order to decide whether chatter has occurred. Using Harmonizer, also the chatter frequency is measured. The frequency at which the energy level exceeds the threshold level is marked as the chatter frequency.

In Fig. 12, the experimental results are compared with the modelled stability lobes. In Fig. 13, the measured chatter frequencies are compared with the modelled chatter frequencies and the natural frequencies of the spindle and tool. It can be concluded that the dynamics of the non-rotating mill highly influences the stability lobes, since the chatter frequency is always close to a resonance frequency of the mill. Clearly, the prediction of the stability lobes diagram is good. Moreover, the

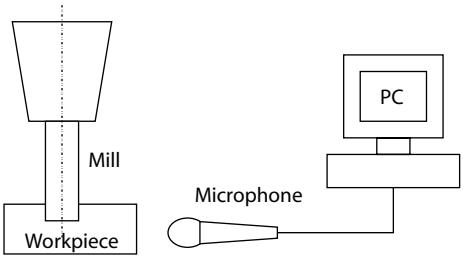

Fig. 11. Experimental setup for the determination of the chatter boundary.

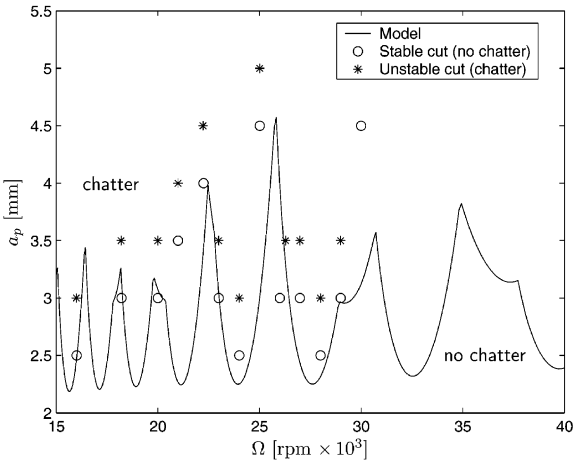

Fig. 12. Modelled stability lobes, compared with experimentally performed cuts.

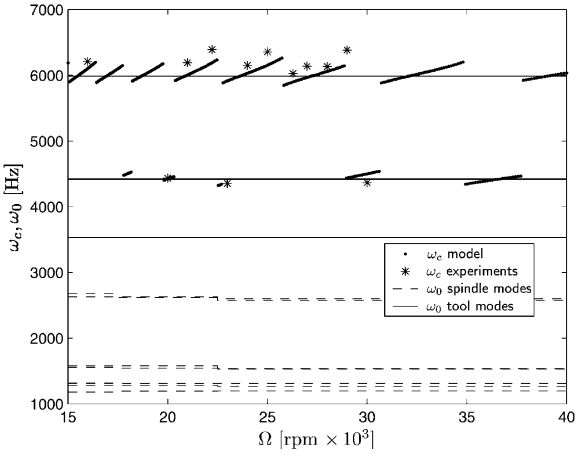

Fig. 13. Chatter frequencies. Asterisks: chatter frequencies in experiments; dots: modelled chatter frequencies; solid lines: natural frequencies of the tool; dashed lines: speed-dependent natural frequencies of the spindle in *x* and *y* direction.

modelled chatter frequencies also resemble the measured chatter frequencies very well. The natural frequencies of the spindle are much lower. This indicates that the dynamics of the spindle, which is spindle speed dependent, is less important than the dynamics of the mill, which is spindle speed independent. It can be concluded that for this specific, rather slender, tool this speed dependency of the spindle dynamics does not influence the stability lobes diagram to a great extent. However, when a shorter, thicker mill would have been used (resulting in extremely high resonance frequencies for the mill dynamics), the spindle dynamics may become dominant. In such a case, the spindle speed dependency of spindle dynamics is important to be included in the stability analysis. The spindle speed dependency of the material parameters causes the minima of the stability lobes to vary with varying spindle speed. With increas-

ing spindle speed, these minima of the stability lobes increase. In order to model this spindle speed dependency, it is necessary to use the method of *D*-partitioning.

5. Conclusions

In this paper, a dynamic model for the milling process has been constructed based on dedicated experiments. Using this model, the stability lobes have been generated. The model, a two-dimensional, linear, higher-order delay-differential equation, includes the following features: (a) an exponential model, in order to model the feed dependency of the stability lobes, (b) spindle speed dependent cutting process parameters, (c) spindle speed dependent machine dynamics.

For the total model, the method of *D*-partitioning is be used to generate the stability lobes. An advantage of this method over the method used by Altintas [1] is that while using the method of *D*-partitioning the critical depth-of-cut can be found for a specific spindle speed, whereas while using the method of Altintas the critical depth-of-cut for a specific chatter frequency, which is an unknown response variable, is found. This allows us, in case of the method of *D*-partitioning, to account for spindle speed dependencies of the milling model, whereas this is not possible in the method of Altintas.

The location of the peaks of the stability lobes, constructed using the model, are in good agreement with the experimentally determined stability limits. However, the model structurally predicts the stability limit slightly too conservative. Chatter frequencies predicted using the model coincide within 3% with the chatter frequencies measured in practice.

Future improvements of the model should account for a helix angle of the cutter. Furthermore, the approximation of the matrix $\underline{k}(t)$ by its zero-th order Fourier approximation (16) can be extended to higher-order approximations, to improve the accuracy of the model. Another issue that will be considered in the future, is the possible time-dependency of the delay parameter τ. However, these latter two changes will demand a different analysis method, since the set of differential equations will be non-autonomous.

References

[1] Y. Altintas, Manufacturing Automation, Cambridge University Press, 2000.
[2] Y. Altintas, E. Budak, Analytical prediction of stability lobes in milling, CIRP Annals 44 (1) (1995) 357–362.
[3] B. Balachandran, M.X. Zhao, A mechanics based model for study of dynamics of milling operations, Meccanica 35 (2000) 89–109.
[4] M.A. Davies, T.J. Burns, C.J. Evans, On the dynamics of chip formation in machining hard materials, CIRP Annals 46 (1997) 25–30.
[5] I. Grabec, Chaotic dynamics of the cutting process, International Journal Machine Tools and Manufacture 28 (1988) 19–32.
[6] T. Insperger, G. Stépán, Stability of the milling process, Periodica Polytechnica Mechanical Engineering 44 (1) (2000) 47–57.
[7] O. Kienzle, H. Victor, Spezifische Schnittkrafte bei der Metallbearbeitung, Werkstofftechnik und Machinenbau 47 (5) (1957) 224–225.
[8] H.Z. Li, X.P. Li, Modeling and simulation of chatter in milling using a predictive force model, International Journal of Machine Tools and Manufacture 40 (2000) 2047–2071.
[9] Manufacturing Laboratories, Inc. Available from http://www.mfg-labs.com.
[10] H.E. Merrit, Theory of self-excited machine tool chatter, Journal of Engineering for Industry 87 (1965) 447–454.
[11] E.P. Nosyreva, A. Molinari, Analysis of nonlinear vibrations in metal cutting, International Journal of Mechanical Sciences 40 (8) (1998) 735–748.
[12] B. Porter, Stability Criteria for Linear Dynamical Systems, Oliver & Boyd, 1967.
[13] G. Stépán, Retarded Dynamical Systems: Stability and Characteristic Functions, Longman, 1989.
[14] G. Stépán, Delay-differential equation models for machine tool chatter, in: F.C. Moon (Ed.), Dynamics and Chaos in Manufacturing Processes, Wiley, 1998, pp. 162–192.
[15] G. Stépán, Modelling nonlinear regenerative effects in metal cutting, Philosophical Transactions of the Royal Society London 359 (A) (2001) 739–757.
[16] J. Tlusty, Manufacturing Processes and Equipment, Prentice Hall, 2000.
[17] J. Tlusty, M. Polacek, The stability of machine tools against self-excited vibrations in machining, Proceedings of the ASME International Research in Production Engineering, Pittsburgh, USA, (1963) 465-474.
[18] S.A. Tobias, Machine Tool Vibration, Blackie, 1965.
[19] S.A. Tobias, W. Fishwick, The chatter of lathe tools under orthogonal cutting conditions, Transaction of the ASME 80 (1958) 1079–1088.
[20] M. Wiercigroch, Nonlinear dynamics of orthogonal metal cutting, in: M. Wiercigroch, A. de Kraker (Eds.), Applied Nonlinear Dynamics and Chaos of Mechanical Systems with Discontinuities, World Scientific, 2000, pp. 361–401.
[21] M. Wiercigroch, E. Budak, Sources of nonlinearities, chatter generation and suppression in metal cutting, Philosophical Transactions of the Royal Society of London 359 (A) (2001) 663–693.
[22] M. Wiercigroch, A.M. Krivtsov, Frictional chatter in orthogonal metal cutting, Philosophical Transactions of the Royal Society of London 359 (A) (2001) 713–738.